Biomacromolecules

Article

Cite This: Biomacromolecules 2018, 19, 132−140

pubs.acs.org/Biomac

Lipogels for Encapsulation of Hydrophilic Proteins and Hydrophobic Small Molecules

Celia C. Homyak,[†] Ann Fernandez,[†] Mollie A. Touve,[‡] Bo Zhao,[†] Francesca Anson,[†] Jeanne A. Hardy,[†,§,⊥] Richard W. Vachet,[†,§,⊥] Nathan C. Gianneschi,[‡,#] Jennifer L. Ross,*[,§,⊥,∥] and S. Thayumanavan*[,†,§,⊥]

[†]Department of Chemistry, [§]Molecular and Cellular Biology Graduate Program, [⊥]Center for Bioactive Delivery, and [∥]Department of Physics, Institute for Applied Life Sciences University of Massachusetts, Amherst, Massachusetts 01003, United States

[‡]Department of Chemistry, Northwestern University, Evanston, Illinois 60208, United States

[#]Department of Chemistry and Biochemistry, University of California, San Diego, La Jolla, California 92093, United States

Supporting Information

ABSTRACT: Lipid−polymer hybrid materials have the potential to exhibit enhanced stability and loading capabilities in comparison to parent liposome or polymer materials. However, complexities lie in formulating and characterizing such complex nanomaterials. Here we describe a lipid-coated polymer gel (lipogel) formulated using a single-pot methodology, where self-assembling liposomes template a UV-curable polymer gel core. Using fluorescently labeled lipids, protein, and hydrophobic molecules, we characterized their formation, purification, stability, and encapsulation efficiency via common instrumentation methods such as dynamic light scattering (DLS), matrix-assisted laser desorption ionization-mass spectrometry (MALDI-MS), UV−vis spectroscopy, fluorescence spectroscopy, and single-particle total internal reflection fluorescence (TIRF) microscopy. In addition, we confirmed that these dual-guest-loaded lipogels are stable in solution for several months. The simplicity of this complete aqueous formation and noncovalent dual-guest encapsulation holds potential as a tunable nanomaterial scaffold.

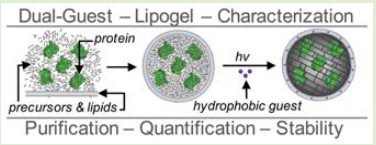

INTRODUCTION

Liposomes (LS) are one of the few marketed nanomedicines found in a vast number of preclinical and clinical technologies for an array of therapies (e.g., vaccines, cancer, gene therapy).[1−3] The aqueous self-assembly, hydrophobic/hydrophilic guest encapsulation, and tunable properties (i.e., size, surface functionality) make LSs advantageous carriers for multiguest delivery. Despite their promise, LSs display subpar in vivo stability and there is a general lack of controlled guest release mechanisms.[1]

As useful alternatives to LSs, polymer nanomedicines can be easily tailored for high stability in vivo. In addition, polymeric materials can be tuned to control guest release under specific biologically relevant stimuli such as pH, redox, or temperature.[4−8] An array of polymeric nanomaterials have reached preclinical trials, but their clinical success has been hindered as polymer biocompatibilities are not yet fully understood.[6] Benefits of clinically relevant LS systems (with dual-guest loading capabilities) along with more stable and tunable polymer nanomaterials (with controllable guest release) have caused a spike in interest to form hybrid lipid−polymer materials.[9−12] Such systems hold great potential due to their enhanced properties when compared to parent LS or polymer materials.

Lipogels are lipid-coated polymer gels and have been of recent interest due to their aqueous self-assembling characteristics and ability to trap hydrophilic and hydrophobic molecules within their aqueous core and lipophilic shell, respectively.[9,11,13−21] Moreover, the separately tunable characteristics of the lipid shell and polymer core allows for a dual-responsive character in which core/shell guests can be selectively released in response to different biologically relevant stimuli.

Lipogels are commonly formed in a one- or two-step process.[13] In the two-step method, hydrophilic guest-loaded polymer gels are initially formed, typically via oil-in-water emulsion. After purification, gels are then coated with a hydrophobic guest-loaded lipid bilayer shell.[21,22] In the one-step LG formation process, an aqueous self-assembling LS is utilized to simultaneously encapsulate polymer precursors and guests. The lipid shell acts as a template for polymerizing the precursors into a cross-linked gel core. Additionally, both hydrophilic (within the core) and hydrophobic (within lipid bilayer) guests can be noncovalently entrapped throughout this process (Scheme 1). Thus, one-step LG formation processes are more appealing due to their simplicity and complete aqueous self-assembly.

Recent efforts have reported LG systems with various polymer, lipid, and guest components.[9−24] The array of lipids and/or guest molecules utilized in these reports has shed light on methods used for particle/guest formation, purification, and characterization. Despite some common trends in formation and purification steps, the complex nature of dual-guest-loaded

Received: September 8, 2017
Revised: November 10, 2017
Published: November 15, 2017

DOI: 10.1021/acs.biomac.7b01300
Biomacromolecules 2018, 19, 132−140

Scheme 1. Single-Pot Method of LG Formation via Liposomal Templating and Subsequent Core Cross-Linking under UV Irradiation[a]

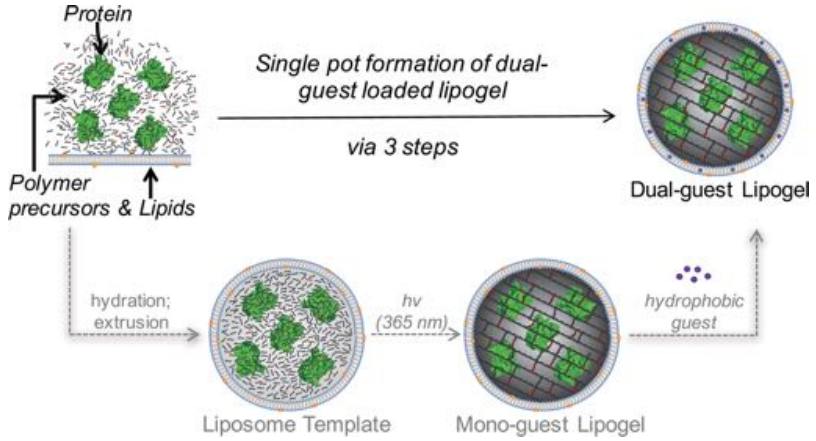

[a]Throughout the LG formation, protein and hydrophobic guests can be noncovalently entrapped within the polymer nanogel core and lipid bilayer shell, respectively.

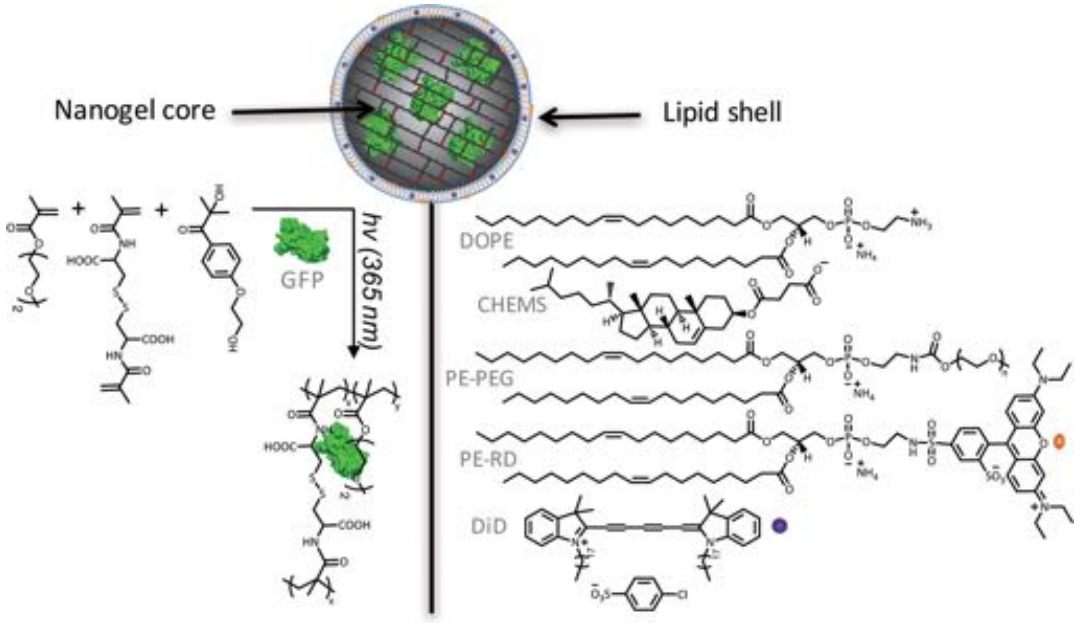

Figure 1. Molecular design for polymer nanogel core with protein guest (left) and lipid shell with hydrophobic small molecule guests (right).

core−shell LG systems makes their characterization a formidable challenge. Establishing common characterization techniques, applicable to a diverse array of LG systems, is necessary for comparing system-to-system variations to develop a better fundamental understanding of LG materials.

Within this work, we report the formation and characterization of a new LG system using a single-pot methodology, which utilized three formation steps. First, both hydrophilic protein and polymer precursors were entrapped within self-assembling LS templates. Second, UV irradiation was used to polymerize the nanosized (100−200 nm) polymer core, which we refer to as a "nanogel". The final step in the formation process is addition of hydrophobic guest, which sequestered within the lipid bilayer shell (Scheme 1). We used labeled lipids and model guest molecules for characterization, allowing system translation for future combinations including therapeutic guests. To track the LG carrier, a rhodamine-labeled phosphoethanolamine lipid (PE-RD) was utilized. In addition, green fluorescent protein (GFP) and hydrophobic dye probes (DiI and DiD) were used for modeling characterization of protein and hydrophobic small molecule guests, respectively. Using multicolor fluorescence detection and imaging we were able to quantify the effectiveness of guest encapsulation within this LG formulation.

EXPERIMENTAL SECTION

Materials. 2-(2-Methoxyethoxy)ethyl methacrylate (DEGM), 2-hydroxy-4′-(2-hydroxyethoxy)-2-methylpropiophenone (IRGACURE 2959, (PI)), sodium-L-ascorbic acid (AA), sodium hydroxide (NaOH), 1,1′-dioctadecyl-3,3,3′,3′-tetramethylindocarbocyanine perchlorate (DiI), carbonic anhydrase (CA), and Triton X-100 (TX) were all purchased from Sigma-Aldrich. 1,1′-Dioctadecyl-3,3,3′,3′-tetramethylindodicarbocyanine perchlorate (DiD) was purchased from ThermoFisher Scientific. Phospholipids and sterol, 1,2-dioleoyl-*sn*-glycero-3-phosphoethanolamine (DOPE), 1,2-dioleoyl-*sn*-glycero-3-phosphoethanolamine-*N*-(lissamine rhodamine B sulfonyl) ammonium salt (PE-RD), 1,2-dioleoyl-*sn*-glycero-3-phosphoethanolamine-*N*-[methoxy-

DOI: 10.1021/acs.biomac.7b01300
Biomacromolecules 2018, 19, 132−140

(polyethylene glycol)-2000] ammonium salt (PE-PEG), and cholesterol hemisuccinate (CHEMS) were purchased from Avanti Polar Lipids Inc. All listed reagents obtained were used without further purification unless otherwise stated.

Methods. Methods of formation, purification, and analysis were performed in pH 7.4, 10 mM PBS buffer, and concentrations are reported with respect to lipid concentration unless otherwise noted. All size analysis was done using dynamic light scatting (DLS) on a Malvern Zetasizer Nano ZS. Bulk sample UV−visible (UV−vis) absorption was monitored on a PerkinElmer Lambda 35 spectrometer, while bulk fluorescence analysis was performed on a PerkinElmer LS 55 spectrometer.

Liposome (LS) Formation. LS formation was done with a total lipid concentration of 2.5 mM, respective to the hydration volume. Lipid composition contained 1% PE-PEG (0.070 mg, 0.025 μmol) with DOPE:CHEMS at a ratio of 60:40 [DOPE (1.1 mg, 1.5 μmol) and CHEMS (0.49 mg, 1.0 μmol)]. Rhodamine-labeled LSs contained additional 0.025% PE-RD (0.81 μg, 0.63 nmol) to the above lipid mixtures (Figure 1). Lipid and sterol components were mixed in chloroform and vortexed before removing $CHCl_3$ under an argon stream and dried under vacuum overnight. Dried lipid films were then hydrated with 1 mL of PBS or polymer precursor hydrant (described below) at 2−8 °C for 3 h, vortexing initially and every hour throughout the hydration period. Following hydration, LSs were extruded 21 times through a polycarbonate membrane (100 nm, 19 mm) using a miniextruder set (Avanti Polar Lipids Inc.). Crude LS templates (cLS) were either directly converted into lipogels (described below) or purified via dialysis (biotech cellulose ester membrane MWCO 300 kDa, Spectrum Laboratories) in PBS at 2−8 °C.

Lipogel (LG) Formation. LG formation utilized lipid films described in the LS formation section above. Dried lipid films were hydrated with a 5% (w/v) (50 mg/mL) polymer precursor solution containing 95% monomer (DEGM) and 5% cross-linker (*N*,*N*′-bis(methacryloyl)-L-cystine (CDM)). CDM was synthesized following a previously reported method and can be found in the Supporting Information (S0).[25] DEGM (44 μL, 125 μmol), CDM (5 mg, 6.6 μmol), PI (0.2 mg, 0.9 μmol), NaOH (50 μL, 1 M), and PBS (0.5 mL) were sonicated to fully disperse reagents followed by dilution with the remaining PBS buffer (0.5 mL) or, in the case of protein-loaded LGs, enhanced green fluorescent protein (GFP) (0.5 mL, 100 μM) or CA (0.5 mL, 100 μM) were added. GFP was expressed in *E. coli* and purified using high-performance liquid chromatography, which is described in more detail in the Supporting Information (S1). Precursor and protein solutions were used to hydrate lipid films and extrude as described in the LS formation section. Crude LSs (cLS) were then mixed with ascorbic acid (AA) (200 mol % with respect to PI), exposed to UV light (365 nm, 30 min), and syringe filtered (0.45 μm pore size) to yield the crude lipogel (cLG). For samples with hydrophobic cargo loading DiI or DiD (0.5 or 10 mol % with respect to lipid) in acetone (≤4% acetone in water) was added to cLGs. After stirring overnight at 2−8 °C, cLGs were syringe filtered before dialysis purification. All cLSs and cLGs were purified via dialysis (biotech cellulose ester membrane MWCO 300 kDa, Spectrum Laboratories) in PBS buffer at 2−8 °C for at least 24 h. Purified liposome (LS) and lipogel (LG) samples were stored at 2−8 °C until further use. Size analysis was done for LSs and LGs (50 μM) both initially and after lipid shell removal with TX (100 mol % with respect to lipid).

Bare Nanogel (NG). Bare nanogel was obtained from cLGs. The lipid shell was removed with TX (100 mol % with respect to lipid) at room temperature for 1−2 h. TX-lipid (TX-L) mixed micelles were then removed via dialysis in PBS (biotech cellulose ester membrane MWCO 100 kDa, Spectrum Laboratories) for 48 h to yield the NG. Size and fluorescence were monitored throughout the purification to confirm removal of lipid micelles from bare NG core.

Cryogenic Electron Microscopy (CryoEM). CryoEM grids were prepared by pipetting 4 μL of sample onto a Quantifoil R2/2 TEM grid that had previously been glow discharged using an Emitech K350 glow discharge unit and plasma cleaned for 90 s in an E.A. Fischione 1020 unit. The grids were blotted with filter paper under high humidity to create thin films and then rapidly plunged into liquid ethane. The grids were stored under liquid nitrogen and then imaged on a FEI Tecnai G2 Sphera microscope operating at 200 keV. The samples were kept at <−175 °C while imaging. Micrographs were recorded on a 2k × 2k Gatan CCD camera.

Matrix-Assisted Laser Desorption Ionization-Mass Spectrometry (MALDI-MS). MALDI-MS analysis was done on free CA and CA-LGs, which were digested and analyzed for the presence of CA peptide fragments. Sample digestion and MALDI-MS analysis were done following our previously reported protocol.[8] In general, CA samples were prepared in 50 mM Tris buffer at pH 8.0.[8] The stock solutions were denatured with 10% acetonitrile at 55 °C for 15 min. After samples were cooled down, immobilized trypsin was added and incubated at 37 °C for 15 h to finish digestion. Samples were then centrifuged at 14 000 rcf to obtain the supernatant as the final CA protein digest solution. Digested samples were analyzed by MALDI-MS with a matrix solution of α-cyano-4-hydroxycinnamic acid (CHCA) prepared at a concentration of 10 mg/mL in 50 μL of ACN, 47.5 μL of H_2O, and 2.5 μL of TFA. MALDI-MS was analyzed on a Bruker Autoflex III time-of-flight mass spectrometer and a Bruker UltrafleXtreme MALDI-TOF/TOF mass spectrometer. All mass spectra were acquired in reflectron mode with an accelerating voltage of 19 kV. Each spectrum is the average of 500 laser shots at 50% power.

Total Internal Reflection Fluorescence (TIRF) Microscopy. TIRF microscopy was performed in three colors to characterize individual LGs with RD, GFP, and/or DiD (0.5% loading). Samples were flowed into glass chambers made from a cover glass, slide treated under UV-ozone for 20 min, and assembled into a flow chamber with double-stick tape. Sample was diluted to 0.5−5 μM with PBS in order to observe physically separated LGs on the glass surface. Free GFP was imaged at 0.01−0.1 nM in PBS as a control to check imaging conditions and photobleaching of single fluorophores. LGs with GFP, RD, and DiD signals were detected using 488, 532, and 638 nm wavelength lasers, respectively. TIRF was performed on a home-built, multilaser system constructed around a Nikon Ti-E inverted microscope equipped with a 60×, 1.49 numerical aperture, oil-coupled objective (Nikon). An additional 4× or 2.5× magnifier was added to make the pixel size 67.5 nm/pixel or 108 nm/pixel, respectively. Images of single LGs in each color were separately recorded using an Andor iXon Duo-648 EMCCD camera. Continuous imaging without shuttering was performed at exposure times of 300−500 ms for 5 min in order to photobleach the GFP signal. The number of GFP molecules in individual LGs was determined by analyzing the GFP intensity over time using the ImageJ software, which is described in detail within the Supporting Information[26] (S5).

Hydrophobic Guest Quantification. Hydrophobic guest quantification was done by UV−vis analysis in acetone. Purified DiI-LGs and DiD-LGs (20−40 μL) were diluted to a final concentration of 50 μM lipid in acetone (1 mL) and syringe filtered (0.45 μm pore size) before checking the absorption. Extracted DiI and DiD in acetone were quantified at λ_{max} absorbance of 549 and 645 nm, respectively. Standard curve calibrations for molar extinction coefficients of DiI and DiD in acetone are shown within the Supporting Information (S4).

Bulk Fluorescence Protein Quantification. Bulk fluorescence protein quantification of GFP-loaded LGs (GFP-LGs) was done via fluorescence spectroscopy. Purified GFP-LGs were diluted to a final concentration of 100 μM lipid in PBS and fluorescence emission monitored for samples and standards at an excitation of 480 nm and scanning speed of 500 nm/min. A linear fit calibration curve of free GFP was made at λ_{max} emission of 522 nm for calculating GFP concentration in bulk GFP-LG solution (S5).

Förster Resonance Energy Transfer (FRET). FRET analysis was done to monitor LG stability. LGs loaded with either 10 mol % DiI (DiI-LG) or 10 mol % DiD (DiD-LG) were mixed in a 1:1 ratio with a final LG concentration of 1−2 mM. Aliquots of the mixture were removed and diluted to 25−50 μM in PBS for each UV−vis and fluorescence reading over a 24 h period. FRET of donor (DiI) and acceptor (DiD) emissions was monitored after an excitation of 480 nm. DLS of cLG and LG samples were also checked with and without TX to ensure LG size and core cross-linking were unaffected (S6).

DOI: 10.1021/acs.biomac.7b01300
Biomacromolecules 2018, 19, 132−140

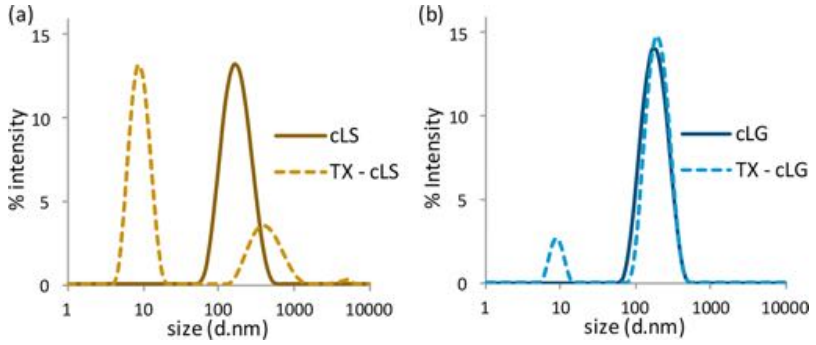

Figure 2. Size analysis of (a) crude liposome (cLS) and (b) crude lipogel (cLG) before and after lipid displacement via TX to confirm LS templating and nanogel cross-linking.

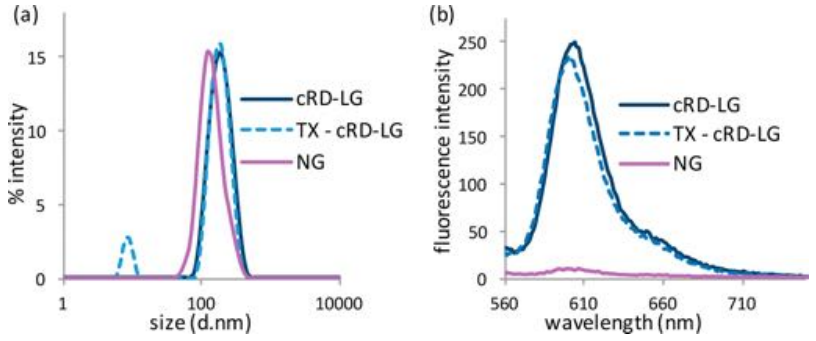

Figure 3. (a) Size of initial LG, lipid-removed LG (LG + TX), and NG after TX-L micelle removal. (b) Fluorescence of RD lipid signal on LG and LG + TX samples but loss of RD signal in pure NG after TX-L removal.

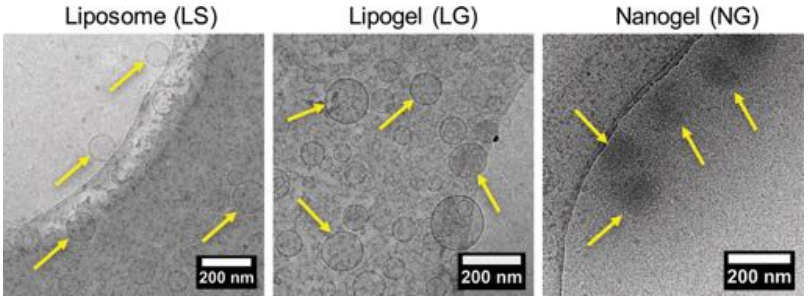

Figure 4. CryoEM images show the morphology of the lipid bilayer observed in LS (left) and LG (middle) samples, while only polymer aggregates are detected with NG (right).

RESULTS AND DISCUSSION

Single-pot LG formation was done using LS templates composed of DOPE and CHEMS with a small amount of poly(ethylene glycol)-functionalized lipid (PE-PEG), which is known to enhance LS stability and biocompatibility (Figure 1).[27] In order to track the lipid shell of LGs a small amount of rhodamine-labeled lipid, PE-RD, was added to specific LG samples. Initial preparation was done through hydration of dried lipid films with an aqueous polymer precursor solution containing 95% monomer (DEGM) and 5% cross-linker (CDM) along with photoinitiator (Figure 1). Protein loading was accomplished by adding either GFP or CA to the polymer precursor solution prior to lipid hydration. Following LS hydration, extrusion was done to aid in polymer precursor and protein encapsulation as well as to ensure monodisperse sizing of LS templates (cLS). The nanogel core was then polymerized within cLSs using UV irradiation to form crude lipogels (cLGs). Similar to reported methods, a photoinhibitor, AA, was added before UV exposure, which prevented polymerization from occurring outside of LS templates.[12,18] After polymer core cross-linking, cLGs were loaded with hydrophobic guest molecules, DiI or DiD. Upon mixing with aqueous LGs DiI and DiD became soluble, which confirmed they were being sequestered within the hydrophobic lipid bilayer shell. All cLSs and cLGs were purified via dialysis to remove any unencapsulated small molecules or proteins.

Characterization of LS templating was first done via size comparisons of cLSs vs their subsequent cLGs. Size similarity between cLS and cLG verified the LS shell acted as a template for the polymer core, and no polymer cross-linking occurred outside of the LS template. Nanogel core cross-linking was confirmed after lipid shell displacement of cLS and cLG samples with TX. When adding TX to cLSs, displacement of lipid occurred to form TX-L mixed micelles (~10 nm). However, when TX is added to cLGs, TX-L mixed micelles (~10 nm) are present along with the cross-linked NG core (~150 nm). These results confirm the presence of cross-linked nanogels inside the liposomes (Figure 2).

DOI: 10.1021/acs.biomac.7b01300
Biomacromolecules 2018, 19, 132−140

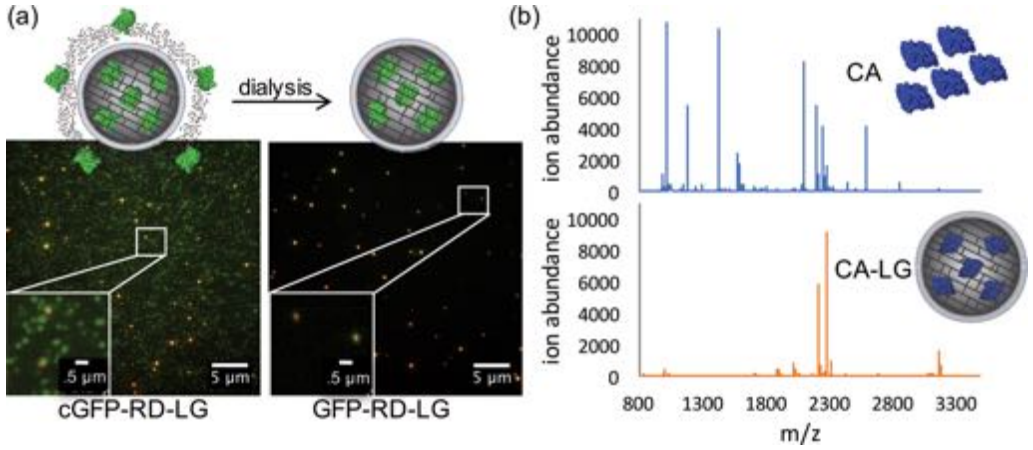

Figure 5. (a) Confirmation of unencapsulated GFP removal via TIRF comparison of GFP-RD lipogels of both crude (cGFP-RD-LG) and pure (GFP-RD-LG). (b) MALDI-MS confirmation of unencapsulated protein removal by comparing peptide fragment signals of free protein (top), which were no longer present within pure CA-LG (bottom). Residual peaks found within the CA-LG sample, corresponding to the empty LG, are shown in the Supporting Information (S3).

To obtain the bare nanogel (NG), TX was used to displace the lipid shell of crude rhodamine-labeled LG (cRD-LG). After TX lipid shell displacement, the TX-L mixed micelles were successfully removed via dialysis to obtain the bare NG. Size was monitored to confirm removal of TX-L micelles (~10 nm) and the remaining NG core (~150−200 nm). Due to excess TX addition, DLS plots are shown in % intensity vs diameter size (nm). Full DLS analysis of this purification is described in more detail in the Supporting Information (S2). The pure NG displayed a similar size to its parent LG sample, further confirming the lipid shell dictated the NG core size. Fluorescence was also monitored to show the initial presence of RD-labeled lipid and the subsequent loss of signal after NG purification, which confirmed the lipid shell was fully removed from the NG (Figure 3).

Morphologies of LS, LG, and NG were characterized by CryoEM. Size distributions of LS, LG, and NG samples from CryoEM images corresponded to sizes observed with bulk DLS analysis. Additionally, unilamellar lipid shell morphology was observed with both LSs and LGs, with minimal changes in size and morphology between the two. Unlike LSs and LGs, the NGs did not have lipid shell coatings but rather existed primarily as polymer aggregates. Differences between LS/LG and NG morphology was additional confirmation that the lipid shell was removed from LGs, as described earlier. (Figure 4).

Typically centrifuge filtration,[24] chromatography,[18] and dialysis[9,10,16] methods are used for purifying LGs. Despite this array of purification techniques, few reports confirm the final purity of LGs to reassure guest molecules were fully encapsulated inside LGs. Since proteins can be entrapped within but also remain free in the solution after LS/LG formation, it was crucial to confirm removal of unencapsulated protein and more importantly to verify that the only remaining protein was trapped within the LGs. Some reports confirm free protein removal and subsequent encapsulation with enzyme activity[10] or protein quantitification[9] assays of LG variations. Due to substrate specificity of activity assays and LS turbidity interference with absorbance-based quantification assays, it was advantageous to explore additional methods for characterizing LG purity and protein encapsulation. Herein, we decided to use two different techniques for such characterization, applicable to an array of fluorescently labeled or enzyme digestible guests, via fluorescence microscopy or mass spectrometry, respectively.

Total internal reflection (TIR) of light occurs when the angle of incidence of a light ray is greater than the critical angle respective to the interface between materials of low- and high-refractive index, such as water and glass.[28] In TIR, a laser beam is reflected at the cover glass−water interface to form an evanescent wave of light that penetrates the sample for only 100−300 nm. This allows materials adhered to the cover glass surface to be easily detected with minimal background signal interferance.[28] Since individual fluorophores are visible on the surface, TIRF microscopy allows visualization of free guest molecules even at parts per billion (nM) concentrations. Using TIRF, we monitored the purity of the LGs through direct visualization of rhodamine-labeled LG (RD-LG, 532 nm) and guest protein (GFP, 488 nm). Prior to dialysis purification, the crude GFP-loaded RD-LG (cGFP-RD-LG) had excess GFP signal in comparison to the RD-LG signal (Figure 5a). After purification, excess GFP was removed and the remaining GFP and RD signals were primarily colocalized, respective to individual GFP-RD-LGs (Figure 5a). Separated GFP and RD images from GFP-RD-LGs can be found in the Supporting Information (S3). Additional analysis of GFP photobleaching was also done with TIRF to quantify protein encapsulation, which is discussed in more detail below. Beyond TIRF, MALDI-MS was also used to verify removal of free protein from pure LGs.

MALDI-MS detection of proteins within polymer nanogel solutions was previously established within our group.[8] Briefly, free or exposed (on exterior of nanoparticle) proteins are subject to digestion from trypsin, a serine protease. If digested proteins are above femtomolar concentrations, their subsequent peptide fragments are detectable by MALDI-MS. Alternatively, if proteins are completely entrapped within the polymer nanoparticle they will not be subject to trypsin digestion and in return negligible on MALDI-MS. For our studies, carbonic anhydrase (CA) was used in place of GFP for such analysis due to CA's similar size to GFP but greater sensitivity to proteolytic digestion. Free CA, along with CA-loaded and purified LG (CA-LG), were digested with trypsin for MALDI-MS peptide fragment analysis. Results revealed peptide fragments corresponding to free CA were negligible (or below femtomolar

DOI: 10.1021/acs.biomac.7b01300
Biomacromolecules 2018, 19, 132−140

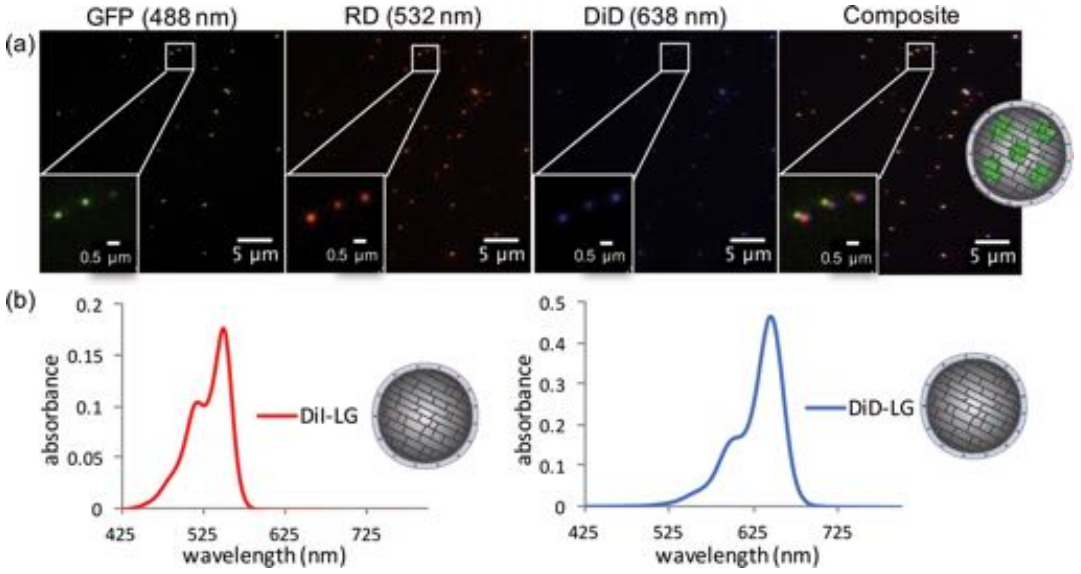

Figure 6. (a) TIRF assessment of dual-guest encapsulation via monitoring GFP (488 nm), RD (532 nm), and DiD (638 nm) colocalization. (b) UV−vis spectra of DiI-LG and DiD-LG for quantification of hydrophobic guest within bulk LG solutions. Standards for DiI/DiD quantification can be found in the Supporting Information (S4).

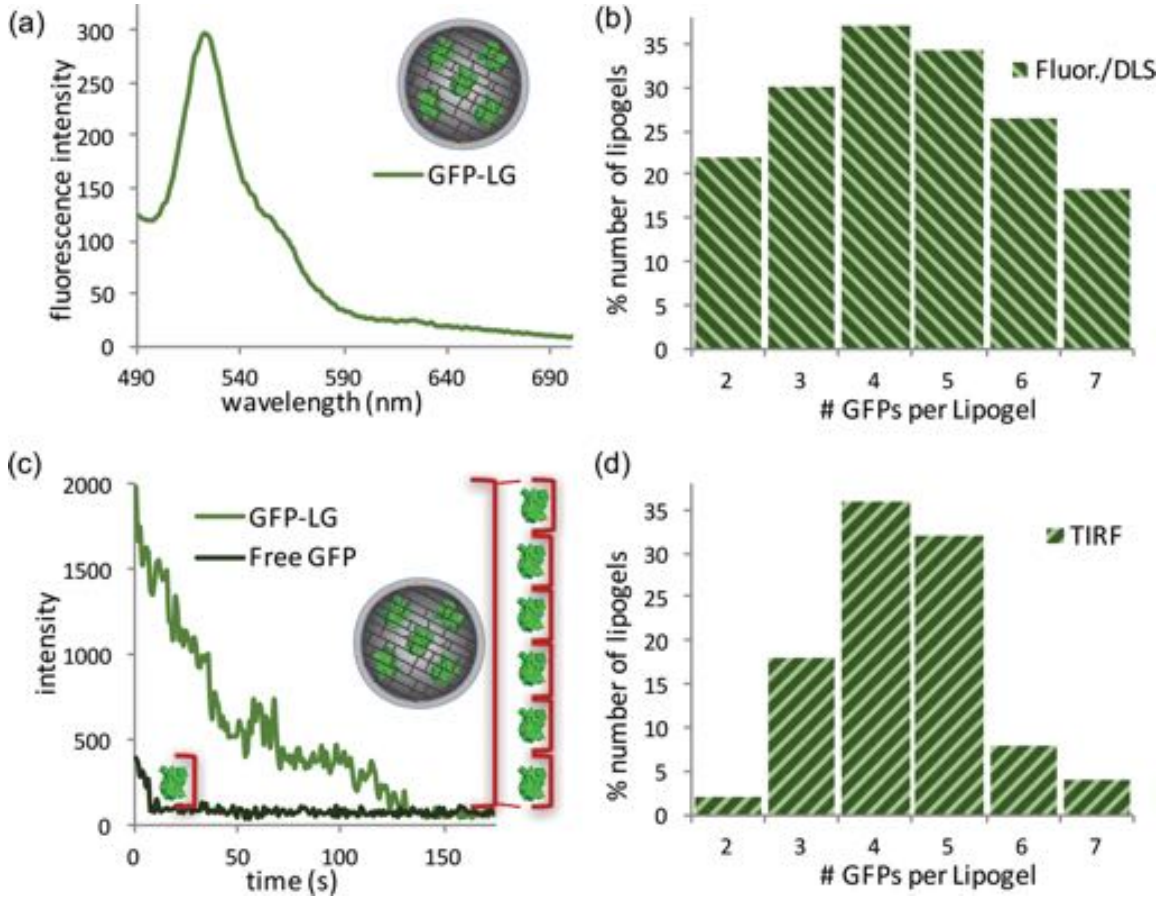

Figure 7. (a) Bulk fluorescence emission of GFP-LG for quantifying GFP molarity, which was used in combination with DLS size and known lipid concentration to determine the number of GFP molecules per LG ($N_{GFP/lipo}$). (b) Distribution of $N_{GFP/lipo}$ throughout bulk samples via fluorescence and DLS analysis. (c) Photobleaching of free GFP (single-step) vs GFP-LG (multistep) confirmed multiple GFP molecules were encapsulated in each LG. (d) Distribution of $N_{GFP/lipo}$ from TIRF photobleaching analysis. Methods to calculate $N_{GFP/lipo}$ for both fluorescence/DLS (Fluor./DLS) and TIRF can be found in the Supporting Information (S5).

concentration) within CA-LGs. The results from MALDI-MS and TIRF analysis show that free proteins were successfully removed after dialysis purification, and the remaining protein molecules are encapsulated within LGs. (Figure 5b)

DOI: 10.1021/acs.biomac.7b01300
Biomacromolecules 2018, 19, 132−140

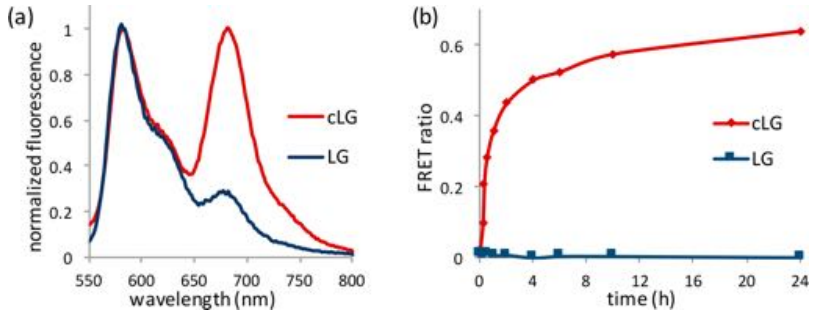

Figure 8. (a) Fluorescence of cLG displaying FRET from donor (DiI, 582 nm) to acceptor (DiD, 681 nm) confirming hydrophobic guest exchange between LGs. (b) FRET ratio over time of cLGs and pure LGs revealed hydrophobic guest exchange occurs before dialysis, while purified samples have minimal to no guest exchange over time.

In addition to free GFP removal, TIRF was also used to verify dual-guest encapsulation within LGs. Similar to the GFP-RD-LG (Figure 5a), the purified DiD-loaded GFP-RD-LG (DiD-GFP-RD-LG) displayed signal for the lipid (RD, 532 nm), protein (GFP, 488 nm), and hydrophobic guest (DiD, 638 nm). Colocalization of individual RD, GFP, and DiD signals within the composite overlay verified both protein and hydrophobic guest were indeed within LGs (Figure 6a). We also confirmed dual-guest encapsulation using UV−vis spectroscopy and fluorimetry of bulk samples.

Quantification of hydrophobic guest within the lipid membrane was done by UV−vis absorption analysis of DiI-LG and DiD-LG samples (Figure 6b). Due to the poor solubility of hydrophobic guests in water, UV−vis quantification was done in acetone for DiI/DiD-LGs and DiI/DiD standard solutions. The amount of DiI and DiD within LGs was quantified using extinction coefficients at λ_{max} values of 549 and 645 nm, respectively (S4). Encapsulation efficiencies of guest amounts in relation to initial amount of guest loaded were 66 ± 5% and 55 ± 4% for DiI and DiD, respectively. Loading efficiency for the amount of guest encapsulated in relation to total lipid concentration was 7 ± 1% and 6 ± <1% for DiI and DiD, respectively. Due to interference from LG turbidity, similar UV−vis analysis was not reliable for GFP quantification. Instead, we were able to quantify GFP using two other methods based on bulk fluorescence and single-particle TIRF.

Quantification of GFP via bulk fluorescence emission of GFP-LGs (Figure 7a) was more feasible than absorbance spectroscopy due to minimal fluorescence interference from LG turbidity. The relative molarity of GFP (M_{GFP}) within GFP-LGs was found using a linear standard curve monitoring emission λ_{max} of 522 nm after 480 nm excitation (S5). Calculated M_{GFP} was then used in combination with DLS size distribution and lipid concentration to determine the number of GFPs per lipogel ($N_{GFP/lipo}$). Plotting the $N_{GFP/lipo}$ with respect to the number of LGs (determined from DLS results) gave the $N_{GFP/lipo}$ distribution, revealing $N_{GFP/lipo}$ of ∼4−5 being the most abundant (Figure 7b). Parameters for these calculations followed literature reports[29−32] and are described in more detail in the Supporting Information (S5). To verify the accuracy of this bulk fluorescence quantification method we also used single-particle TIRF to quantify $N_{GFP/lipo}$ for individual LGs.

Additional quantification of GFP inside individual LGs was done by GFP photobleaching in TIRF microscopy using the 488 nm laser.[26] Individual LGs are diffraction limited in fluorescence imaging, but the fluorescence intensity reveals the number of fluorophores in a diffraction-limited region as long as the intensity falls within the linear range of the detector. We also used purified single GFP molecules as a control and internal calibration standard. GFP molecules and LGs were imaged continuously over time. Analysis of the intensity of individual fluorescent spots displayed significantly different photobleaching patterns for free GFP and GFP-LGs. As expected, free GFP spots had single-step photobleaching patterns. Alternatively, GFP-LG spots (of the same size as free GFP) had a higher initial fluorescence intensity which decayed via a multistep GFP photobleaching pattern, implying that there were multiple GFP molecules in each LG (Figure 7c). Photobleaching patterns for individual spots within many GFP-LG samples were further analyzed to determine $N_{GFP/lipo}$. The distribution of $N_{GFP/lipo}$ was compiled from individual GFP-LG spot analyses. In agreement with fluorescence quantification, TIRF quantification revealed $N_{GFP/lipo}$ of ∼4−5 being the most abundant overall (Figure 7d). Similarities in $N_{GFP/lipo}$ abundance for fluorescence and TIRF quantification methods validated the utility of these two quantification methods (Figure 7b and 7d). In addition to guest quantifying guest encapsulation, we also established methods to easily monitor LG shell stability.

Common encapsulation and stability analysis of guests within lipid bilayer systems is done by tracking hydrophilic guest molecule release (e.g., fluorescent self-quenching hydrophilic guest, dialysis membrane diffusion) or monitoring FRET of covalently labeled lipid pairs.[27] Due to their insolubility in aqueous medium, such methods are not applicable to quantifying encapsulation/release of hydrophobic guest molecules. To selectively monitor hydrophobic guest encapsulation and release for tracking lipid bilayer stability we decided to use a different reported method[33] which instead tracks the hydrophobic guest concentration and exchange overtime using UV−vis and FRET. By using LGs loaded with either fluorescent donor (DiI) or acceptor (DiD) molecules, their exchange over time could be monitored by FRET. When DiI and DiD are in close proximity, FRET occurs, which implies leakage from one lipid shell to another. If the DiI and DiD guests are stably encapsulated within the lipid shell then there should be no FRET detected. DiI-LG and DiD-LG samples were made separately and then mixed to monitor any change in FRET ratio. Analysis of this was done by plotting the FRET ratio $I_a/(I_d + I_a)$ vs time, where I_a and I_d are the maximum emission intensity of the acceptor (DiD) and the donor (DiI) at 681 and 582 nm, respectively, measured separately. Full fluorescence spectra for all FRET analyses can be found in the Supporting Information. With all FRET analyses, the UV−vis absorption was also monitored to confirm that guest molecule

DOI: 10.1021/acs.biomac.7b01300
Biomacromolecules 2018, 19, 132−140

concentration remained the same despite changes in the FRET ratio (S6).

Initial fluorescence analysis of crude LG (cLG) and pure LG (LG) samples revealed they had significantly different lipid shell stabilities (Figure 8a). Minimal to no FRET exchange over time was detected with LGs, which reassured LGs have little to no leakage in solution and maintain stably encapsulated hydrophobic guests (Figure 8b). Interestingly, cLGs, which contain polymer precursors, displayed an opposite FRET ratio trend over time (Figure 8b). Despite the increasing FRET ratio, hydrophobic guest absorption was maintained over time (S6). This provided reassurance that the lipid shell was still present in cLGs, although not stable enough to fully trap hydrophobic guest molecules. Additional DLS analysis of cLGs and LGs confirmed that particle size and core cross-linking were also unaffected, despite differences in lipid destabilization (S6).

To determine the cause of instability within the cLGs, an additional FRET analysis was performed after reintroducing monomer and cross-linker into purified LGs. The resulting FRET ratio did increase in comparison to the LG, which verified that small molecule polymer precursors were causing lipid shell instability (S7). This phenomenon confirmed that the hydrophobicity of DiI and DiD had minimal effect on lipid shell stability, while precursor small molecules had a much larger effect on encapsulation stability. Overall, the lipid shell of LGs is significantly stabilized to maintain hydrophobic guest loading after dialysis purification. In addition, size and core cross-linking of LGs were checked again after 3 months of storage at 2−8 °C. Both LG size and core cross-linking were well maintained after storage, which further verified the solution stability of these LGs (S8).

CONCLUSIONS

In this work, we established a single-pot method for the formation for dual-guest-loaded lipogels. A number of characterization techniques have been brought to bear analysis of these lipogels, from their initial formation to their final stability. All these techniques have applicability with a variety of LG systems containing diverse lipid, protein, and/or hydrophobic small molecule components. Initial formation was characterized by DLS before and after lipid shell displacement. Purification of LGs was monitored using TIRF and MALDI-MS to ensure full removal of any unencapsulated guest molecules. Hydrophobic guest quantification was executed via UV−vis absorption spectroscopy, while protein encapsulation was quantified using bulk fluorimetry and single-particle TIRF analyses. Monitoring FRET of mixed LGs over time along with size analysis after 3 months confirmed these LGs have excellent solution stability after purification. Overall, the noncovalent dual-guest encapsulation capability of LGs holds potential to surpass current nanomaterial systems, which commonly require specific carrier−guest interactions and/or excess synthetic effort for such encapsulation capabilities. Additionally, the tunable core/shell properties of this LG system provide means for controlling material stability and functionality in addition to selective release of hydrophobic or hydrophilic guest molecules. To the best of our knowledge, a dual-guest-loaded system that also harnesses core/shell dual responsivity has yet to be done with current LG scaffolds. With that results reported here are being pursued in more detail to understand the stimuli-sensitive characteristics of these LGs along with their viability under more biologically relevant conditions.

ASSOCIATED CONTENT

Supporting Information

The Supporting Information is available free of charge on the ACS Publications website at DOI: 10.1021/acs.biomac.7b01300.

Further experimental methods and data analyses (PDF)

AUTHOR INFORMATION

Corresponding Authors

*E-mail: thai@chem.umass.edu (S. T.).
*E-mail: rossj@physics.umass.edu (J. R.).

ORCID

Jeanne A. Hardy: 0000-0002-3406-7997
Richard W. Vachet: 0000-0003-4514-0210
Nathan C. Gianneschi: 0000-0001-9945-5475
S. Thayumanavan: 0000-0002-6475-6726

Notes

The authors declare no competing financial interest.

ACKNOWLEDGMENTS

This research was conducted with financial support from the U.S. Army Research Office (W911NF-15-1-0568), partial support from NCI of the National Institutes of Health (CA-169140), the NIH Biotechnology Training Program for F.A. (GM108556), and from the Air Force Office of Scientific Research, National Defense Science and Engineering Graduate (NDSEG) Fellowship, 32 CFR 168a, to M.A.T. TEM analysis of materials was conducted at the UCSD Cryo-Electron Microscopy Facility, supported by NIH funding to Dr. Timothy S. Baker and the Agouron Institute gifts to UCSD.

REFERENCES

(1) Grimaldi, N.; Andrade, F.; Segovia, N.; Ferrer-Tasies, L.; Sala, S.; Veciana, J.; Ventosa, N. Lipid-Based Nanovesicles for Nanomedicine. *Chem. Soc. Rev.* **2016**, *45*, 6520−6545.

(2) Anselmo, A. C.; Mitragotri, S. Nanoparticles in the Clinic. *Bioeng. Transl. Med.* **2016**, *1* (4), 10−29.

(3) Pattni, B. S.; Chupin, V. V.; Torchilin, V. P. New Developments in Liposomal Drug Delivery. *Chem. Rev.* **2015**, *115*, 10938−10966.

(4) Karimi, M.; Ghasemi, A.; Sahandi Zangabad, P.; Rahighi, R.; Moosavi Basri, S. M.; Mirshekari, H.; Amiri, M.; Shafaei Pishabad, Z.; Aslani, A.; Bozorgomid, M.; et al. Smart Micro/nanoparticles in Stimulus-Responsive Drug/gene Delivery Systems. *Chem. Soc. Rev.* **2016**, *45*, 1457−1501.

(5) Torchilin, V. P. Multifunctional, Stimuli-Sensitive Nanoparticulate Systems for Drug Delivery. *Nat. Rev. Drug Discovery* **2014**, *13* (11), 813−827.

(6) Homyak, C.; Anson, F.; Thayumanavan, S. Supramolecular Polymers in Nanomedicine. In *Comprehensive Supramolecular Chemistry II*; Atwood, J. L., Ed.; Elsevier, 2017; Vol. *5*, pp 227−254.

(7) Molla, M. R.; Marcinko, T.; Prasad, P.; Deming, D.; Garman, S. C.; Thayumanavan, S. Unlocking a Caged Lysosomal Protein from a Polymeric Nanogel with a pH Trigger. *Biomacromolecules* **2014**, *15* (11), 4046−4053.

(8) Ventura, J.; Eron, S. J.; González-Toro, D. C.; Raghupathi, K.; Wang, F.; Hardy, J. A.; Thayumanavan, S. Reactive Self-Assembly of Polymers and Proteins to Reversibly Silence a Killer Protein. *Biomacromolecules* **2015**, *16* (10), 3161−3171.

(9) Lockhart, J. N.; Beezer, D. B.; Stevens, D. M.; Spears, B. R.; Harth, E. One-Pot Polyglycidol Nanogels via Liposome Master Templates for Dual Drug Delivery. *J. Controlled Release* **2016**, *244*, 366−374.

(10) Bobone, S.; Miele, E.; Cerroni, B.; Roversi, D.; Bocedi, A.; Nicolai, E.; Di Venere, A.; Placidi, E.; Ricci, G.; Rosato, N.; et al.

DOI: 10.1021/acs.biomac.7b01300
Biomacromolecules 2018, 19, 132−140

Liposome-Templated Hydrogel Nanoparticles as Vehicles for Enzyme-Based Therapies. *Langmuir* **2015**, *31*, 7572−7580.
(11) Liang, Y.; Kiick, K. L. Multifunctional Lipid-Coated Polymer Nanogels Crosslinked by Photo-Triggered Michael-Type Addition. *Polym. Chem.* **2014**, *5* (5), 1728−1736.
(12) Schillemans, J. P.; Flesch, F. M.; Hennink, W. E.; van Nostrum, C. F. Synthesis of Bilayer-Coated Nanogels by Selective Cross-Linking of Monomers inside Liposomes. *Macromolecules* **2006**, *39* (17), 5885−5890.
(13) Krishnamurthy, S.; Vaiyapuri, R.; Zhang, L.; Chan, J. M. Lipid-Coated Polymeric Nanoparticles for Cancer Drug Delivery. *Biomater. Sci.* **2015**, *3*, 923−936.
(14) Kiser, P. F.; Wilson, G.; Needham, D. Lipid-Coated Microgels for the Triggered Release of Doxorubicin. *J. Controlled Release* **2000**, *68* (1), 9−22.
(15) Campbell, A.; Taylor, P.; Cayre, O. J.; Paunov, V. N. Preparation of Aqueous Gel Beads Coated by Lipid Bilayers. *Chem. Commun.* **2004**, *44* (21), 2378−2379.
(16) Saleem, Q.; Liu, B.; Gradinaru, C. C.; Macdonald, P. M. Lipogels: Single-Lipid-Bilayer-Enclosed Hydrogel Spheres. *Biomacromolecules* **2011**, *12* (6), 2364−2374.
(17) Lu, N.; Yang, K.; Li, J.; Weng, Y.; Yuan, B.; Ma, Y. Controlled Drug Loading and Release of a Stimuli-Responsive Lipogel Consisting of Poly (N - Isopropylacrylamide) Particles and Lipids. *J. Phys. Chem. B* **2013**, *117*, 9677−9682.
(18) Wang, Y.; Tu, S.; Pinchuk, A. N.; Xiong, M. P. Active Drug Encapsulation and Release Kinetics from Hydrogel-in-Liposome Nanoparticles. *J. Colloid Interface Sci.* **2013**, *406*, 247−255.
(19) Stolzoff, M.; Ekladious, I.; Colby, A. H.; Colson, Y. L.; Porter, T. M.; Grinstaff, M. W. Synthesis and Characterization of Hybrid Polymer/Lipid Expansile Nanoparticles: Imparting Surface Functionality for Targeting and Stability. *Biomacromolecules* **2015**, *16*, 1958−1966.
(20) Raemdonck, K.; Braeckmans, K.; Demeester, J.; De Smedt, S. C. Merging the Best of Both Worlds: Hybrid Lipid-Enveloped Matrix Nanocomposites in Drug Delivery. *Chem. Soc. Rev.* **2014**, *43* (1), 444−472.
(21) Zhang, L.-J.; Wu, B.; Zhou, W.; Wang, C.-X.; Wang, Q.; Yu, H.; Zhuo, R.-X.; Liu, Z.-L.; Huang, S.-W. Two-Component Reduction-Sensitive Lipid−polymer Hybrid Nanoparticles for Triggered Drug Release and Enhanced in Vitro and in Vivo Anti-Tumor Efficacy. *Biomater. Sci.* **2017**, *5* (1), 98−110.
(22) Park, J.; Wrzesinski, S. H.; Stern, E.; Look, M.; Criscione, J.; Ragheb, R.; Jay, S. M.; Demento, S. L.; Agawu, A.; Licona Limon, P.; et al. Combination Delivery of TGF-β Inhibitor and IL-2 by Nanoscale Liposomal Polymeric Gels Enhances Tumour Immunotherapy. *Nat. Mater.* **2012**, *11* (10), 895−905.
(23) Murrieta-Pazos, I.; Gaiani, C.; Galet, L.; Cuq, B.; Desobry, S.; Scher, J. Comparative Study of Particle Structure Evolution during Water Sorption: Skim and Whole Milk Powders. *Colloids Surf., B* **2011**, *87* (1), 1−10.
(24) Pohlit, H.; Bellinghausen, I.; Schömer, M.; Heydenreich, B.; Saloga, J.; Frey, H. Biodegradable pH-Sensitive Poly(ethylene Glycol) Nanocarriers for Allergen Encapsulation and Controlled Release. *Biomacromolecules* **2015**, *16*, 3103−3111.
(25) Andac, M.; Plieva, F. M.; Denizli, a.; Galaev, I. Y.; Mattiasson, B. Poly(hydroxyethyl Methacrylate)-Based Macroporous Hydrogels with Disulfide Cross-Linker. *Macromol. Chem. Phys.* **2008**, *209* (6), 577−584.
(26) Ross, J. L.; Dixit, R. Multiple Color Single Molecule TIRF Imaging and Tracking of MAPs and Motors. In *Methods in Cell Biology, Microtubules in vitro*; Correia, J., Wilson, L., Eds.; Academic Press, 2010; pp 521−542.
(27) Vanić, Z.; Barnert, S.; Süss, R.; Schubert, R. Fusogenic Activity of PEGylated pH-Sensitive Liposomes. *J. Liposome Res.* **2012**, *22* (2), 148−157.
(28) Colomb, W.; Sarkar, S. K. Extracting Physics of Life at the Molecular Level: A Review of Single-Molecule Data Analyses. *Phys. Life Rev.* **2015**, *13*, 107−137.
(29) Sardan, M.; Kilinc, M.; Genc, R.; Tekinay, A. B.; Guler, M. O. Cell Penetrating Peptide Amphiphile Integrated Liposomal Systems for Enhanced Delivery of Anticancer Drugs to Tumor Cells. *Faraday Discuss.* **2013**, *166*, 269−283.
(30) Ding, W.; Palaiokostas, M.; Wang, W.; Orsi, M. Effects of Lipid Composition on Bilayer Membranes Quantified by All-Atom Molecular Dynamics. *J. Phys. Chem. B* **2015**, *119* (49), 15263−15274.
(31) Brzozowska, I.; Figaszewski, Z. A. The Equilibrium of Phosphatidylcholine-Cholesterol in Monolayers at the Air/water Interface. *Colloids Surf., B* **2002**, *23* (1), 51−58.
(32) Duncanson, W. J.; Figa, M. A.; Hallock, K.; Zalipsky, S.; Hamilton, J. A.; Wong, J. Y. Targeted Binding of PLA Microparticles with Lipid-PEG-Tethered Ligands. *Biomaterials* **2007**, *28* (33), 4991−4999.
(33) Jiwpanich, S.; Ryu, J.; Bickerton, S.; Thayumanavan, S. Noncovalent Encapsulation Stabilities in Supramolecular Nanoassemblies. *J. Am. Chem. Soc.* **2010**, *132* (31), 10683−10685.

DOI: 10.1021/acs.biomac.7b01300
Biomacromolecules 2018, 19, 132−140